5

Dynamics at Low Magnetic Reynolds Numbers

> It was perhaps for the advantage of science that Faraday, though thoroughly conscious of the forms of space, time and force, was not a professed mathematician. He was not tempted to enter into the many interesting researches in pure mathematics... and he did not feel called upon either to force his results into a shape acceptable to the mathematical taste of the time, or to express them in a form which the mathematicians might attack. He was thus left to his proper work, to coordinate his ideas with his facts, and to express them in natural, uncomplicated language.
>
> *Maxwell (1873)*

In Chapter 4 we looked at the effect of fluid motion on a magnetic field without worrying about the back reaction of **B** on **u**. We now consider the reverse problem, in which **B** influences **u** (via the Lorentz force), but **u** does not significantly perturb **B**. In short, we look at the effect of a prescribed magnetic field on the flow. To ensure that **B** remains unaffected by **u** we must restrict ourselves to low magnetic Reynolds numbers:

$$R_m = ul/\lambda = \mu\sigma ul \ll 1 \tag{5.1}$$

However, this is not overly restrictive, at least not in the case of liquid-metal MHD. For example, in most laboratory experiments, or industrial processes, $\lambda \sim 1\ \mathrm{m}^2/\mathrm{s}$, $l \sim 0.1$ m and internal friction keeps **u** to a level of around 0.01 m/s $\rightarrow$ 1 m/s. This gives $R_m \sim 0.001 \rightarrow 0.1$. The only exception is dynamo theory, where the large length scales involved result in $R_m \sim 100$. We also note in passing that the viscosity, ν, of liquid metal is similar to that of water, and so the Reynolds numbers of most liquid-metal flows is very high.

Now a magnetic field can alter **u** in three ways. It can suppress bulk motion, excite bulk motion, or alter the structure of the boundary layers in some way. We look at the first of these possibilities in Part 1, where we discuss the damping of flows using a static magnetic field. We tackle the second possibility in Part 2, where the effect of a rotating magnetic field is investigated. Finally, we examine boundary layers (Hartmann layers) in Part 3. We start, however, with the governing equations of low-R_m MHD.

5.1 The Low-R_m Approximation in MHD

The essence of the low-R_m approximation is that the magnetic field associated with induced currents, $\mathbf{J} \sim \sigma \mathbf{u} \times \mathbf{B}$, is negligible by comparison with the imposed magnetic field. There are three distinct cases which commonly arise.

(i) The imposed magnetic field is static, the flow is induced by some external agency, and friction keeps $\mathbf{u}$ to a modest level in the sense that $|\mathbf{u}| \ll \lambda/l$.

(ii) The imposed magnetic field travels or rotates uniformly and slowly such that $\mathbf{u}_{\text{field}} \ll \lambda/l$. This induces a flow $\mathbf{u}$ which, due to friction in the fluid, is somewhat slower than the speed of the field.

(iii) The imposed magnetic field oscillates extremely rapidly, in the sense that the skin-depth $\delta = (2/\mu\sigma\omega)^{1/2}$ is much less than l, ω being the field frequency. The magnetic field is then excluded from the interior of the conductor (see Section 4.5) and inertia or friction in the fluid ensures that $|\mathbf{u}| \ll \omega l$.

Categories (i)–(iii) cover the majority of flows in engineering applications. Typical examples are the magnetic damping of jets, vortices or turbulence (case (i)), magnetic stirring using a rotating magnetic field (case (ii)) and magnetic levitation (case (iii)). We shall leave the discussion of flows of type (iii) until Chapter 12. Here we focus on cases (i) and (ii).

Now if the imposed magnetic field travels or rotates in a uniform manner, then a suitable change of frame of reference will convert problems of type (ii) into those of type (i). Without loss of generality, therefore, we may take $\mathbf{B}$ to be steady.

We now discuss the simplifications which result in the governing equations when R_m is low and the imposed magnetic field is steady. Let $\mathbf{E}_0$, $\mathbf{J}_0$ and $\mathbf{B}_0$ represent the fields which would exist in a given situation if $\mathbf{u} = 0$, and let $\mathbf{e}$, $\mathbf{j}$ and $\mathbf{b}$ be the infinitesimal perturbations in $\mathbf{E}$, $\mathbf{J}$ and $\mathbf{B}$ which occur due to the presence of a vanishingly small velocity field. These quantities are governed by

$$\nabla \times \mathbf{E}_0 = 0, \qquad \mathbf{J}_0 = \sigma \mathbf{E}_0 \tag{5.2a, b}$$

$$\nabla \times \mathbf{e} = -\partial \mathbf{b}/\partial t, \qquad \mathbf{j} = \sigma(\mathbf{e} + \mathbf{u} \times \mathbf{B}_0) \tag{5.3a, b}$$

where we have neglected the second-order term $\mathbf{u} \times \mathbf{b}$ in (5.3b). Now Faraday's equation gives $\mathbf{e} \sim \mathbf{ub}$ and so the perturbation in the electric field may also be neglected in (5.3b). Ohm's law now becomes

$$\mathbf{J} = \mathbf{J}_0 + \mathbf{j} = \sigma(\mathbf{E}_0 + \mathbf{u} \times \mathbf{B}_0)$$

However, $\mathbf{E}_0$ is irrotational and so may be written as $-\nabla V$, where V is an electrostatic potential. Our final version of Ohm's law is therefore

$$\boxed{\mathbf{J} = \sigma(-\nabla V + \mathbf{u} \times \mathbf{B}_0)} \tag{5.4}$$

while the leading-order term in the Lorentz force (per unit volume) is

$$\boxed{\mathbf{F} = \mathbf{J} \times \mathbf{B}_0} \tag{5.5}$$

Equations (5.4) and (5.5) are all that we require to evaluate the Lorentz force in low-R_m MHD. There is no need to calculate $\mathbf{b}$ since it does not appear in the Lorentz force. Moreover, $\mathbf{J}$ is uniquely determined by (5.4) since

$$\nabla \cdot \mathbf{J} = 0, \qquad \nabla \times \mathbf{J} = \sigma \nabla \times (\mathbf{u} \times \mathbf{B}_0) \tag{5.6a, b}$$

and a vector field is unambiguously determined if its divergence and curl are known (and some suitable boundary conditions are specified).

From now on we shall drop the subscript on $\mathbf{B}_0$, on the understanding that $\mathbf{B}$ represents the imposed, steady magnetic field.

Part 1: Suppression of Motion

5.2 Magnetic Damping

There are many industrial and laboratory processes in which an intense, static magnetic field is used to suppress unwanted motion in a liquid metal. For example, in the continuous casting of large steel slabs, an intense DC magnetic field ($\sim 10^4$ Gauss) is commonly used to suppress motion within the mould. Sometimes the motion takes the form of a submerged jet which feeds the mould from above, at others it takes the form of large vortices. In both cases the aim is to keep the free surface of the liquid quiescent, thus avoiding the entrainment of surface debris. Magnetic damping is also used in the laboratory measurements of chemical and thermal diffusivities, particularly where thermal or solutal buoyancy can disrupt the measurement technique. These examples are discussed in more detail in Chapter 9. Here we present just a glimpse of the possibilities offered by magnetic damping. We shall consider the fluid

to be infinite in extent, or else bounded by an electrically insulating surface, S. For simplicity we neglect the viscous forces and take the imposed magnetic field to be uniform.

5.2.1 *The destruction of mechanical energy via Joule dissipation*

To some extent, the mechanism of magnetic damping is clear. Motion across magnetic field lines induces a current. This leads to Joule dissipation and the resulting rise in thermal energy is accompanied by a corresponding fall in kinetic energy. This is evident from (5.4) and (5.5), which give the rate of working of the Lorentz force as

$$(\mathbf{J} \times \mathbf{B}) \cdot \mathbf{u} = -\mathbf{J} \cdot (\mathbf{u} \times \mathbf{B}) = -\left(J^2/\sigma\right) - \nabla \cdot [V\mathbf{J}]$$

while the product of the inviscid equation of motion with $\mathbf{u}$ yields

$$\frac{D}{Dt}\left[\frac{1}{2}\rho\mathbf{u}^2\right] = (\mathbf{J} \times \mathbf{B}) \cdot \mathbf{u} - \nabla \cdot [p\mathbf{u}]$$

Combining the two furnishes the energy equation

$$\frac{d}{dt}\int \frac{1}{2}\rho\mathbf{u}^2 dV = -\frac{1}{\sigma}\int \mathbf{J}^2 dV \tag{5.7}$$

Thus, as anticipated, Joule dissipation leads to a fall in kinetic energy. However, there are other, more subtle effects associated with magnetic damping. Specifically, the action of a magnetic field is anisotropic. It opposes motion normal to the field lines but leaves motion parallel to $\mathbf{B}$ unopposed. Moreover, as we shall see, vorticity and linear momentum tend to propagate along the field lines by a pseudo-diffusion process. These anisotropic effects can be understood in terms of field sweeping and a Maxwell tension in the $\mathbf{B}$-lines, as discussed in Section 3.9.

For example, consider a jet which is directed at right angles to a uniform magnetic field. Motion across the field lines induces a second, weak, magnetic field. The combined field is then bowed slightly in the direction of $\mathbf{u}$ and the resulting curvature gives rise to a Lorentz force $B^2/\mu R$ which opposes the motion. The tension in the field lines then causes the disturbance to spread laterally along the $\mathbf{B}$-lines.

Now all of this is, to say the least, a little heuristic. However, a couple of simple examples will help establish the general ideas. We start with the jet shown in Figure 5.1.

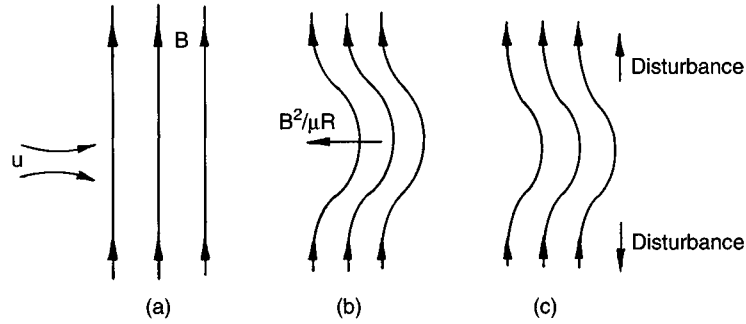

Figure 5.1 Motion across the field lines distorts those lines and the resulting curvature gives rise to a force $B^2/\mu R$ opposing the motion. The disturbance also propagates laterally along the magnetic field lines.

5.2.2 The damping of a two-dimensional jet

The Lorentz force per unit mass acting on the jet shown in Figure 5.1 is, from (5.4),

$$\mathbf{F} = (\mathbf{J} \times \mathbf{B})/\rho = -\mathbf{u}_\perp/\tau - \nabla V \times (\sigma \mathbf{B}/\rho) \tag{5.8}$$

Here $\mathbf{u}_\perp$ represents the velocity components normal to $\mathbf{B}$, and τ is the magnetic damping time, $\tau = (\sigma B^2/\rho)^{-1}$. Note the anisotropic nature of this force. Pressure forces and the effect of V apart, each fluid particle decelerates on a time scale of τ, according to

$$\frac{D\mathbf{u}_\perp}{Dt} \sim -\frac{\mathbf{u}_\perp}{\tau}, \qquad \frac{D\mathbf{u}_{//}}{Dt} \sim 0$$

It is as if each element of fluid which tries to cross a magnetic field line experiences a frictional drag. As a simple example, consider a thin, steady, two-dimensional jet, $\mathbf{u}(x, y) = (u_x, u_y, 0)$, directed along the x-axis and passing through a uniform field imposed in the y-direction. This geometry is particularly easy to handle since both the pressure p and potential V are zero (or constant), as we now show. The divergence of Ohm's law gives

$$\nabla^2 V = \nabla \cdot (\mathbf{u} \times \mathbf{B}) = \mathbf{B} \cdot \boldsymbol{\omega} = 0 \tag{5.9}$$

and so V is zero provided there is no electrostatic field imposed from the boundaries (we exclude such cases). The induced current, $\mathbf{J} = \sigma \mathbf{u} \times \mathbf{B}$, is then directed along the z-axis and the Lorentz force, $\mathbf{J} \times \mathbf{B} = -\sigma u_x B^2 \hat{\mathbf{e}}_x$, acts to retard the flow. Moreover, the fluid surrounding the jet is quiescent and so $\nabla p = 0$ outside the jet. Provided the jet is thin, in the sense that its characteristic thickness, δ, is much less than a characteristic axial

length scale, l, then ∇p is also negligible within the jet. (If the streamlines are virtually straight and parallel then there can be no significant pressure gradients normal to the streamlines.) In this simple example, then, both the pressure forces and $\nabla V \times \mathbf{B}$ are zero. It follows that

$$\mathbf{u} \cdot \nabla u_x = -u_x/\tau \tag{5.10}$$

Equation (5.10) is readily solved. We look for a similarity solution of the form $u_x = u_0(x)f(y/\delta(x))$, where u_0 is the velocity on the axis and $u_0\delta^2$ is constant. Then (5.10) applied to the axis gives $u_0'(x) = -1/\tau$. Next we find u_y using continuity, evaluate $\mathbf{u} \cdot \nabla u_x$, and substitute for this term in (5.10). This yields

$$f^2 - \frac{1}{2}f'(\eta)\int_0^\eta f d\eta = f, \qquad \eta = y/\delta$$

which has solution $f = \text{sech}^2(\eta)$. Thus the velocity distribution in the jet is

$$u_x = [U - x/\tau]\,\text{sec}\,h^2(y/\delta) \tag{5.11}$$

where $U = u_x(0, 0)$. The most striking feature of this solution is that the jet is annihilated within a finite distance $L = U\tau$. The situation is as shown below. Note that our solution ceases to be valid as we approach $x = U\tau$ since $\delta/l \sim \delta/U\tau \sim \delta(0)/(U\tau - x)$, which is not small for $x \sim U\tau$.

We shall return to the topic of MHD jets in Chapter 9, where we look at more complex flows. Interestingly, it turns out that Figure 5.2(a) is quite misleading when it comes to three-dimensional jets. In fact, a three-dimensional jet maintains its linear momentum and so cannot come to a halt. It has the shape shown in Figure 5.2(b).

5.2.3 *Damping of a vortex*

Let us now consider a second example, designed to bring out the tendency for vorticity to diffuse along the magnetic field lines. As before, we take **B** to be uniform. This time, however, we consider the initial velocity field to be an axisymmetric, swirling vortex, $\mathbf{u} = (0, \Gamma/r, 0)$ in (r, θ, z) coordinates. **B** is taken to be parallel to the z-axis. At $t = 0$ the angular momentum per unit mass, $\Gamma(r, z)$, is assumed to be confined to a sphere of size δ, as shown in Figure 5.3(a).

Now the axial gradients in Γ will, via the centrifugal force, tend to induce a poloidal component of motion, $\mathbf{u}_p = (u_r, 0, u_z)$. That is, if Γ is a function of z then the centripetal force, $(\Gamma^2/r^3)\hat{\mathbf{e}}_r$, is rotational and cannot

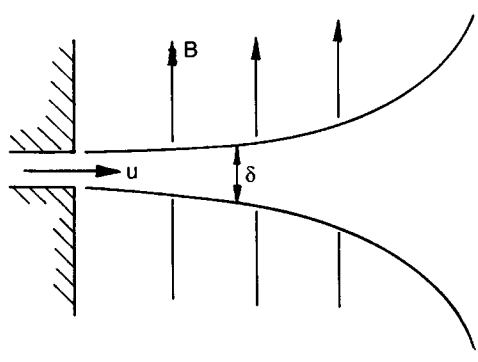

Figure 5.2 (a) A two-dimensional jet is destroyed by a magnetic field in a distance $U\tau$.

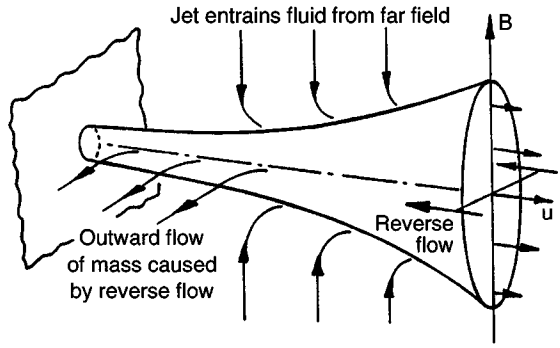

Figure 5.2 (b) A three-dimensional MHD jet.

be balanced by a radial pressure gradient. A secondary, poloidal motion then results which complicates the problem. However, in the interests of simplicity, we shall take $\mathbf{J} \times \mathbf{B} \gg \mathbf{u} \cdot \nabla \mathbf{u}$, which is equivalent to specifying that the magnetic damping time, τ, is much less than the inertial timescale δ/u_0. Since poloidal motion grows on a timescale of δ/u_θ, we may then neglect $\mathbf{u}_p$ for times of order τ.

Let us now determine the induced current, $\mathbf{J}$, and hence the Lorentz force which acts on the (initially) spherical vortex. The term $\mathbf{u} \times \mathbf{B}$ in Ohm's law gives rise to a radial component of current, J_r. However, the current lines must form closed paths and so an electrostatic potential, $V(r, z)$, is established, whose primary function is to ensure that the $\mathbf{J}$-lines close. The distribution of V is in accordance with the first part of (5.9). It

drives an axial component of current, thus allowing **J** to form closed current paths in the r–z plane, as shown in Figure 5.3(a). Since **J** is solenoidal, we can introduce a vector potential defined by

$$\mathbf{J} = \nabla \times [(\phi/r)\hat{\mathbf{e}}_\theta] = \left(-\frac{1}{r}\frac{\partial \phi}{\partial z}, 0, \frac{1}{r}\frac{\partial \phi}{\partial r}\right)$$

In the fluid mechanics literature ϕ would be called the Stokes streamfunction for **J**. For reasons which will become apparent shortly, it is convenient to take the curl of this,

$$\nabla \times \mathbf{J} = -\frac{1}{r}\left(\nabla_*^2 \phi\right)\hat{\mathbf{e}}_\theta$$

where ∇_*^2 is the Laplacian-like operator,

$$\nabla_*^2 \equiv \frac{\partial^2}{\partial z^2} + r\frac{\partial}{\partial r}\left(\frac{1}{r}\frac{\partial}{\partial r}\right)$$

However, Ohm's law (5.6b) gives us $\nabla \times \mathbf{J} = \sigma B \partial \mathbf{u}/\partial z$, and so

$$\nabla_*^2 \phi = -\sigma B \frac{\partial \Gamma}{\partial z} \tag{5.12}$$

We have managed to relate φ, and hence **J,** to the flow field. This allows us to evaluate the Lorentz force per unit mass, $\mathbf{F} = -(J_r B/\rho)\hat{\mathbf{e}}_\theta = F_\theta \hat{\mathbf{e}}_\theta$, in terms of Γ.

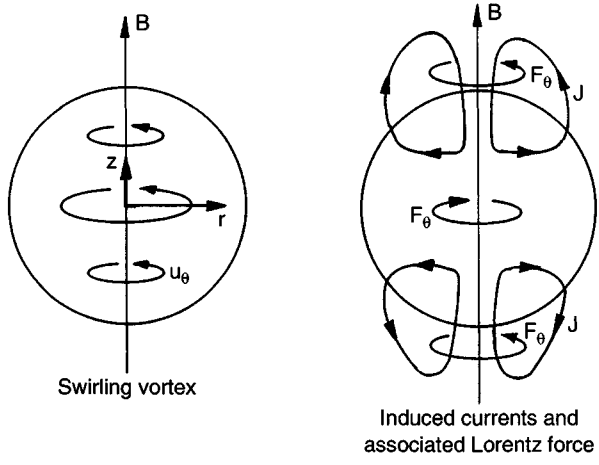

Figure 5.3 (a) An initially spherical vortex is damped by a magnetic field.

$$rF_\theta = \frac{B}{\rho}\frac{\partial \phi}{\partial z} = -\frac{1}{\tau}\frac{\partial^2}{\partial z^2}\left(\nabla_*^{-2}\Gamma\right)$$

Here the inverse operator $f = \nabla_*^{-2}(g)$ is simply a symbolic representation of $\nabla_*^2 f = g$. From Figure 5.3(a) we might anticipate that F_θ is negative in the core of the vortex, decelerating the fluid, and positive above and below the vortex, inducing motion in previously quiesant regions. This, in turn, suggests that Γ spreads along the magnetic field lines. We shall now confirm that this is indeed the case. The azimuthal equation of motion is

$$\frac{D\Gamma}{Dt} = rF_\theta$$

Note that, in the absence of the Lorentz force, angular momentum is materially conserved (i.e. preserved by each fluid particle), there being no azimuthal pressure gradient in an axisymmetric flow. Since we are neglecting the poloidal motion on a timescale of τ, our equation of motion becomes

$$\frac{\partial \Gamma}{\partial t} = \frac{B}{\rho}\frac{\partial \phi}{\partial z} = -\frac{1}{\tau}\frac{\partial^2}{\partial z^2}\left(\nabla_*^{-2}\Gamma\right) \tag{5.13}$$

The first thing to note from (5.13) is that the global angular momentum, H, of the vortex is conserved:

$$\frac{dH}{dt} = \frac{d}{dt}\int \Gamma dV = \frac{B}{\rho}\int \nabla \cdot [\phi \hat{\mathbf{e}}_z] dV = 0$$

Yet energy is continually dissipated in accordance with (5.7),

$$\frac{dE}{dt} = -\frac{1}{\rho\sigma}\int J^2 dV, \qquad E = \frac{1}{2}\int u^2 dV$$

How can the vortex preserve its angular momentum in the face of continual Joule dissipation? We shall see that the answer to this question holds the key to the evolution of the vortex. Let l_r and l_z be characteristic radial and axial length scales, respectively, for the vortex. At $t = 0$ we have $l_r = l_z = \delta$, and we shall suppose that l_r remains of order δ throughout the life of the vortex, there being no reason to suppose otherwise. (We shall confirm this shortly.) Then (5.6b), in the form $\nabla \times \mathbf{J} = \sigma \nabla \times (\mathbf{u} \times \mathbf{B}_0)$, allows us to estimate the magnitude of $\nabla \times \mathbf{J}$, and hence $\mathbf{J}$, from which

$$\frac{dE}{dt} \sim -\frac{1}{\tau}\left(\frac{\delta}{l_z}\right)^2 E, \qquad E \sim \Gamma^2 l_z \tag{5.14}$$

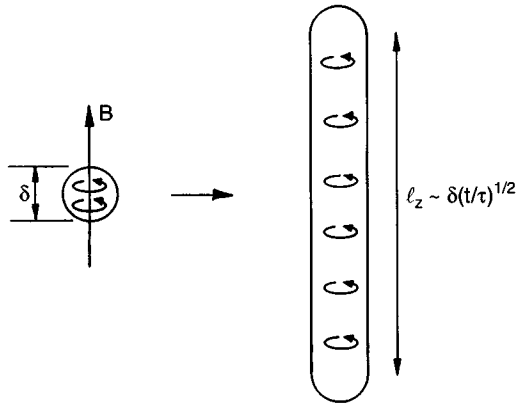

Figure 5.3 (b) Diffusion of angular momentum along the magnetic field lines causes an initially spherical vortex to elongate into a cigar-like shape.

However, we also have

$$H \sim \Gamma \delta^2 l_z = \text{constant} \tag{5.15}$$

It is evident that l_z must increase with time since otherwise E would decay exponentially on a timescale of τ, which contradicts (5.15). In fact the only way of satisfying both (5.14) and (5.15) is when Γ and l_z scale as

$$\Gamma \sim \Gamma_0 (t/\tau)^{-1/2}, \qquad l_z \sim \delta (t/\tau)^{1/2} \tag{5.16}$$

which, in turn, suggests that the kinetic energy of the vortex declines as $(t/\tau)^{-1/2}$. It seems that the vortex evolves from a sphere to an elongated cigar-like shape on a timescale of τ (Figure 5.3(b)). This is the first hint of the pseudo-diffusion process discussed earlier. In fact, we might have anticipated (5.16) from (5.13), written in the form

$$\frac{\partial \Gamma}{\partial t} = -\frac{1}{\tau} \frac{\partial^2}{\partial z^2} \left(\nabla_*^{-2} \Gamma \right) \sim \frac{\delta^2}{\tau} \frac{\partial^2 \Gamma}{\partial z^2} \tag{5.17}$$

suggesting diffusion along the magnetic field lines with a diffusivity of $\alpha_B \sim \delta^2/\tau$. (This argument may be made rigorous by taking Fourier transforms.) Recalling that the diffusion rate in a typical thermal problem is $l \sim \sqrt{\alpha t}$, we have $l_z \sim \delta (t/\tau)^{1/2}$, as in (5.16).

In the spirit of field sweeping and Maxwell tensions, we might picture this diffusion process as a spiralling up of the magnetic field lines, which then slowly unwind, propagating angular momentum along the z-axis. We shall return to this idea in Section 6.1, where we show that this

pseudo-diffusion is the last vestige of Alfvén wave propagation at low R_m. We shall also see, in Chapter 7, that $l_z \sim (t/\tau)^{1/2}$ and $K.E. \sim (t/\tau)^{-1/2}$ characterises MHD turbulence at low R_m, which is perhaps hardly surprising since turbulence just consists of an ensemble of vortices, rather like that shown in Figure 5.3(b).

An exercise for the enthusiastic or the sceptical

The estimates (5.16) may be confirmed by detailed analysis. The most direct method of solving (5.13) is to use Fourier transforms. In axisymmetric problems the three-dimensional Fourier transform reduces to the so-called cosine-Hankel transform, defined by the transform pair

$$F(u_\theta) = U(k_r, k_z) = 4\pi \int_0^\infty \int_0^\infty [u_\theta] J_1(k_r r) \cos(k_z z) r dr dz$$

$$F^{-1}(U) = u_\theta(r, z) = \frac{1}{2\pi^2} \int_0^\infty \int_0^\infty [U] J_1(k_r r) \cos(k_z z) k_r dk_r dk_z$$

This transform has the convenient properties

$$F\left(\partial^2 f/\partial z^2\right) = -k_z^2 F(f), \qquad F(\nabla_*^2 f) = -\left(k_r^2 + k_z^2\right) F(f) = -k^2 F(f)$$

and so the transform of (5.13) is

$$\frac{\partial U}{\partial t} = -\left[\cos^2 \alpha\right] \frac{U}{\tau}, \qquad \cos \alpha = k_z/k$$

Solving for U and performing the inverse transform yields

$$\Gamma = \frac{r}{2\pi^2} \int_0^\infty \int_0^\infty \left[U_0 \exp\left(-\cos^2 \alpha \ (t/\tau)\right)\right] J_1(k_r r) \cos(k_z z) k_r dk_r dk_z$$

where $U_0 = F(u_\theta)$ at $t = 0$. Confirm that for $t \gg \tau$ this integral takes the form

$$\Gamma = (t/\tau)^{-1/2} G(r, z/(t/\tau)^{1/2}) \tag{5.18}$$

where G is determined by the initial condition. Thus confirm that

$$\Gamma \sim (t/\tau)^{-1/2}, \qquad l_z \sim (t/\tau)^{1/2}$$

as suggested earlier on the basis of qualitative arguments. Evidently, the vortex distorts from a sphere to a column, growing axially at a rate $l_z \sim \delta(t/\tau)^{1/2}$. This axial elongation is essential to preserving the angular momentum of the vortex.

5.3 A Glimpse at MHD Turbulence

The last example in Section 5.2 suggests that a turbulent flow evolving in a magnetic field will behave very differently to conventional turbulence, and this is indeed the case. We examine this issue in detail in Chapter 7; here we just give a flavour of some of the underlying ideas. A classic problem in conventional turbulence theory is the so-called free decay of a turbulent flow, and it is worth considering this purely hydrodynamic problem first.

Suppose that the fluid in a large vessel is stirred vigorously and then left to itself. Suppose also that the eddies created by the stirring are randomly orientated and distributed throughout the vessel, so that the initial turbulence is statistically homogeneous and isotropic. Let the vessel have size L and a typical eddy have size l and velocity u. We take $\mathbf{B}$ to be zero and $L \gg l$ so that the boundaries have little influence on the bulk of the motion. The first thing which happens is that some of the eddies which are set up at $t = 0$ break up through inertially driven instabilities, creating a whole spectrum of eddy sizes, from l down to $l_{\min} \sim (ul/\nu)^{-3/4} l$, the latter length scale being the smallest eddy size which may exist in a turbulent flow without being eradicated by viscosity. (Eddies of size $l_{\min}$ are characterised by $\nu\nabla^2\mathbf{u} \sim \mathbf{u} \cdot \nabla\mathbf{u}$ – see Chapter 7.) There then follows a period of decay in which energy is extracted from the turbulence via the destruction of small-scale eddies by viscous stresses, kinetic energy being continually passed down from the large scales to the small scales through the break up of the larger eddies. This 'free decay' process is characterised by the facts that: (i) the turbulence remains approximately homogeneous and isotropic during the decay; (ii) the energy (per unit mass) declines according to Kolmogorov's decay law $E \sim E_0(u_0 t/l_0)^{-10/7}$, or something fairly close to this (u_0 and l_0 are the initial values of u and l). Again, the details are spelled out in Chapter 7.

Now suppose that we repeat this process but in the presence of a uniform magnetic field $\mathbf{B} = B\hat{\mathbf{e}}_z$. For simplicity, we take the fluid to be inviscid and to be housed in a large electrically insulated sphere of radius R, with $R \gg l$ (Figure 5.4(a)). From (5.6b) and (5.7) we have

$$\frac{dE}{dt} = -\frac{1}{\rho\sigma}\int J^2 dV, \qquad E = \frac{1}{2}\int u^2 dV \tag{5.19}$$

$$\nabla \times \mathbf{J} = \sigma B \frac{\partial \mathbf{u}}{\partial z}, \qquad \nabla \cdot \mathbf{J} = 0 \tag{5.20}$$

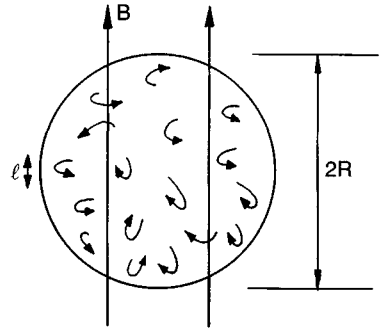

Figure 5.4 (a) Decaying turbulence in a magnetic field.

Clearly the kinetic energy of the flow falls monotonically, and this process ceases if, and only if, **u** is independent of z, i.e. $\mathbf{J} = 0$. However, one component of angular momentum is conserved during this decay. Formally, this may be seen by transforming the expression for the component of torque parallel to **B** as follows:

$$[\mathbf{x} \times (\mathbf{J} \times \mathbf{B})] \cdot \mathbf{B} = [(\mathbf{x} \cdot \mathbf{B})\mathbf{J} - (\mathbf{x} \cdot \mathbf{J})\mathbf{B}] \cdot \mathbf{B} = -(B^2/2)\nabla \cdot \left[x_\perp^2 \mathbf{J}\right] \quad (5.21)$$

This integrates to zero over the sphere (remember that $\mathbf{J} \cdot d\mathbf{S} = 0$). Thus the global Lorentz torque parallel to **B** is zero and so, since there are no viscous forces, one component of angular momentum,

$$\mathbf{H}_{//} = \int (\mathbf{x} \times \mathbf{u})_{//} dV$$

is conserved as the flow evolves. (We take the origin of coordinates to lie at the centre of the sphere and use // and $\perp$ to indicate components of a vector parallel and normal to **B**.) The physical interpretation of (5.21) is straightforward. The current density, **J**, may be considered to be composed of many current tubes, and each of these may, in turn, be considered to be the sum of many infinitesimal current loops, as in the proof of Stokes' theorem. However, the torque on each elementary current loop is $d\mathbf{m} \times \mathbf{B}$, where $d\mathbf{m}$ is its dipole moment, and this is perpendicular to **B**. Consequently, the global torque, which is the sum of many such terms, can have no component parallel to **B**. Conservation of $\mathbf{H}_{//}$ then follows.

As we shall see, this conservation law is fundamental to the evolution of a turbulent flow. In fact, we may show that, as in the last example of Section 5.2, the conservation of $\mathbf{H}_{//}$, combined with continual Joule dissipation, leads to an elongation of the eddies. Let us pursue this idea a little further. Since $\mathbf{H}_{//}$ is conserved, the energy of the flow cannot fall to

zero. Yet (5.20) tells us that **J** is non-zero, and the Joule dissipation finite, as long as **u** is a function of z. It follows that, eventually, the flow must settle down to a two-dimensional one, in which **u** exhibits no variation along the field lines. We may determine how quickly this happens as follows. Noting that the ith component of torque may be written as

$$2[\mathbf{x} \times (\mathbf{J} \times \mathbf{B})]_i = [(\mathbf{x} \times \mathbf{J}) \times \mathbf{B}]_i + \nabla \cdot \left[(\mathbf{x} \times (\mathbf{x} \times \mathbf{B}))_i \mathbf{J}\right] \tag{5.22}$$

we may rewrite the global Lorentz torque in terms of the dipole moment, **m**, of **J**,

$$\mathbf{T} = \int \mathbf{x} \times (\mathbf{J} \times \mathbf{B}) dV = \frac{1}{2} \left\{ \int \mathbf{x} \times \mathbf{J} dV \right\} \times \mathbf{B} = \mathbf{m} \times \mathbf{B}$$

Also, from Ohm's law (5.4), we have

$$(\mathbf{x} \times \mathbf{J}) = \sigma[\mathbf{x} \times (\mathbf{u} \times \mathbf{B}) + \nabla \times (\mathbf{x} V)]$$

(Here V now stands for the electrostatic potential rather than volume.) On integrating this expression over the spherical volume, the second term on the right converts to a surface integral which is zero since $\mathbf{x} \times d\mathbf{S} = 0$. The first contribution on the right may be rewritten (using a version of (5.22) in which **u** replaces **J**) as $\frac{1}{2}(\mathbf{x} \times \mathbf{u}) \times \mathbf{B}$ plus a divergence, which also integrates to zero. It follows that

$$\mathbf{m} = (\sigma/4)\mathbf{H} \times \mathbf{B}$$

and so the global Lorentz torque becomes

$$\mathbf{T} = -\frac{\sigma B^2}{4} \mathbf{H}_\perp$$

The global angular momentum equation

$$\rho \frac{\partial \mathbf{H}}{\partial t} = \mathbf{T} = -\frac{\sigma B^2}{4} \mathbf{H}_\perp$$

then yields

$$\mathbf{H}_{//} = \text{constant}, \qquad \mathbf{H}_\perp = \mathbf{H}_\perp(0) \exp(-t/4\tau) \tag{5.23a, b}$$

As expected, $\mathbf{H}_{//}$ is conserved while $\mathbf{H}_\perp$ decays exponentially on a time scale of τ. The simplicity of this inviscid result is surprising, partially because of its generality (the initial conditions may be quite random), and partially because the local momentum equation

$$\rho \left(\frac{\partial \mathbf{u}}{\partial t} + \mathbf{u} \cdot \nabla \mathbf{u} \right) = -\nabla p + \mathbf{J} \times \mathbf{B}$$

is quadratic in **u** and so possesses analytical solutions only for the most trivial of flows.

Equations (5.23a, b) are highly suggestive. The preferential destruction of $\mathbf{H}_\perp$ suggests that vortices whose axes are perpendicular to **B** are annihilated, leading to a quasi-two-dimensional flow. We may quantify this as follows. First we need the Schwartz integral inequality. In its simplest form this states that any two functions, f and g, satisfy the inequality

$$\left[\int fg dV\right]^2 \leq \int f^2 dV \int g^2 dV$$

The analogous results for arbitrary vector fields **A** and **B** are

$$\left[\int \mathbf{A}\cdot\mathbf{B} dV\right]^2 \leq \int \mathbf{A}^2 dV \int \mathbf{B}^2 dV$$

and

$$\left[\int \mathbf{A}\times\mathbf{B} dV\right]^2 \leq \int \mathbf{A}^2 dV \int \mathbf{B}^2 dV$$

In the present context, this yields

$$\mathbf{H}_{//}^2 \leq \int \mathbf{x}_\perp^2 dV \int \mathbf{u}_\perp^2 dV$$

which, in turn, furnishes a lower bound on the energy, E,

$$E \geq \mathbf{H}_{//}^2 \left[2\int \mathbf{x}_\perp^2 dV\right]^{-1} \tag{5.24}$$

Thus, provided $\mathbf{H}_{//}$ is non-zero, the flow cannot come to rest. Yet (5.20) tells us that, as long as there is some variation of velocity along the **B**-lines, the Joule dissipation remains finite, and E falls. Consequently, whatever the initial condition, the flow must evolve to a steady state that is strictly two-dimensional, exhibiting no variation of **u** along the field lines. In short, the flow adopts the form of one or more columnar vortices, each aligned with the **B**-field (Figure 5.4(b)), all other components of angular momentum being destroyed on a time scale of 4τ. The simplicity of this result is surprising, particularly since it is valid for any value of $u\tau/l$, i.e. unlike the example in Section 5.2, this is valid for any ratio of $|\mathbf{J}\times\mathbf{B}|$ to inertia.

It appears, therefore, that magnetic fields tend to induce a strong anisotropy in a turbulent flow, stretching the eddies in the direction of **B**. Of course, any real fluid is viscous and so this stretching of vorticity will be

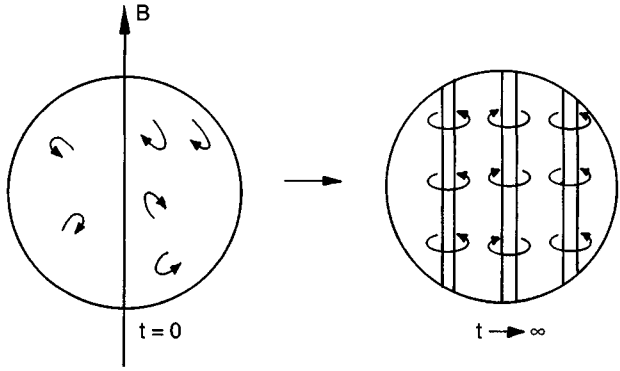

Figure 5.4 (b) MHD turbulences evolve to a two-dimensional state under the influence of pseudo-diffusion.

accompanied by viscous dissipation, just as in conventional turbulence. The eddies become elongated only if they survive for long enough. This, in turn, requires that $\mathbf{J} \times \mathbf{B}$ be at least of order $(\mathbf{u} \cdot \nabla)\mathbf{u}$ and so we would expect strong anisotropy in a real flow only if the interaction parameter $N = l/u\tau$ is greater than unity. We return to this topic in Chapter 7.

5.4 Natural Convection in the Presence of a Magnetic Field

As a final example of the dissipative effect of a static magnetic field we consider the influence of a uniform, imposed field on natural convection. We start with a description of natural convection in the absence of a magnetic field.

5.4.1 Rayleigh–Bénard convection

It is a common experience that a fluid pool heated from below exhibits natural convection. Hot, buoyant, fluid rises from the base of the pool. When this fluid reaches the surface it cools, and sinks back down to the base. Such a flow is characterised by the continual conversion of gravitational energy into kinetic energy, the potential energy being released as light fluid rises and heavy fluid falls. However, this motion is opposed by viscous dissipation, and if the heating is uniform across the base of the pool, and the viscosity high enough, no motion takes place. Rather, the fluid remains in a state of hydrostatic equilibrium and heat diffuses

upwards by conduction alone. The transition between the static, diffusive state and that of natural convection occurs at a critical value of

$$Ra = g\beta\Delta T d^3/\nu\alpha$$

called the Rayleigh number. Here ΔT is the imposed temperature difference between the top and the bottom of the pool, d the depth of the pool, β the expansion coefficient of the fluid (in units of K^{-1}) and α is the thermal diffusivity. The sudden transition from one state to another is called the Rayleigh–Bénard instability, in recognition of Bénard's experimental work in 1900 and the subsequent analytical investigation by Rayleigh in 1916. Rayleigh described Bénard's experiment thus:

> Bénard worked with very thin layers, only about 1 mm deep, standing on a levelled metallic plate which was maintained at a uniform temperature... The layer rapidly resolves itself into a number of 'cells', the motion being an ascension in the middle of a cell and a descension at the common boundary between a cell and its neighbours.

Inspired by these experiments, Rayleigh developed the theory of convective instability for a thin layer of fluid between horizontal planes. He found that the destabilising effect of buoyancy (heavy fluid sitting over light fluid) wins out over the stabilizing influence of viscosity only when Ra exceeds a critical value $(Ra)_c$. For fluid bounded by two solid planes the critical value is 1708, while an open pool with a free upper surface has $(Ra)_c = 1100$. In principle, one can also do the calculation where both the bottom and top surfaces are free (although the physical significance of such a geometry is unclear) and this yields $(Ra)_c = 658$.

Ironically, many years later, it was discovered that the motions observed by Bénard were driven, for the most part, by surface tension, and not by buoyancy. (This is because Bénard used very thin layers.) Nevertheless Rayleigh's analysis of convective instability remains valid. We now extend this analysis to incorporate the stabilising (dissipative) effect of a magnetic field.

5.4.2 The governing equations

When dealing with natural convection in a liquid it is conventional and convenient to use the Boussinesq approximation. In effect, this says that density variations are so small that we may continue to treat the fluid as incompressible and having uniform density, ρ, except to the extent that it introduces a buoyancy force per unit volume, $\delta\rho\mathbf{g}$, into the Navier–Stokes

equation. This buoyancy force is usually rewritten as $-\rho\beta T\mathbf{g}$, where β is the expansion coefficient, $-(\partial\rho/\partial T)/\rho$, and T is the temperature (relative to some datum). The governing equations in the presence of an imposed, vertical field, $\mathbf{B}_0$, are then

$$\frac{D\mathbf{u}}{Dt} = -\nabla\left(\frac{p}{\rho}\right) + \frac{1}{\rho}(\mathbf{J}\times\mathbf{B}_0) + \nu\nabla^2\mathbf{u} - \beta T\mathbf{g}$$

$$\nabla\cdot\mathbf{u} = 0, \qquad \mathbf{J} = \sigma(-\nabla V + \mathbf{u}\times\mathbf{B}_0)$$

$$\frac{DT}{Dt} = \alpha\nabla^2 T$$

Here we have ignored the internal heating due to viscous and Joule dissipation by comparison with the heat transfer from the lower boundary. The stationary configuration whose stability is in question is

$$\mathbf{u}_0 = 0, \qquad T_0 = \Delta T(1 - z/d), \qquad \mathbf{J}_0 = 0$$

Here we take z to point vertically upward, the top and bottom surfaces to lie at $z = 0$ and d, and ΔT is the imposed temperature difference $T(z = 0) - T(z = d)$. Now the formal method of determining the stability of such a base state is straightforward. One looks for slightly perturbed solutions of the form $T = T_0 + \delta T$, $\mathbf{u} = \mathbf{u}_0 + \delta\mathbf{u}$ and $\mathbf{J} = \mathbf{J}_0 + \delta\mathbf{J} = \delta\mathbf{J}$, substitute these into the governing equations, discard terms which are quadratic in the disturbance, and look for separable solutions of the linearised equations in the form $\mathbf{u} = \hat{\mathbf{u}}(\mathbf{x})\exp(jst)$. If all goes well, this results in an eigenvalue problem, the eigenvalues of which determine the growth (or decay) rate of some initial disturbance. This process is long and tedious, resulting in an eighth-order differential system, and we do not intend to do it. Rather, we shall give an heuristic description of the instability which captures the key physics of the process and yields a surprisingly accurate estimate of $(Ra)_c$.

5.4.3 *An energy analysis of the Rayleigh–Bénard instability*

If we take the product of the Navier–Stokes equation with $\mathbf{u}$, we obtain

$$\frac{\partial}{\partial t}\left(\frac{u^2}{2}\right) = -\nabla\cdot\left[\left(\frac{p}{\rho} + \frac{u^2}{2}\right)\mathbf{u}\right] + \frac{1}{\rho}(\mathbf{J}\times\mathbf{B}_0)\cdot\mathbf{u} - \nu(\mathbf{u}\cdot(\nabla\times\boldsymbol{\omega})) + g\beta T u_z$$

The rate of working of the Lorentz, viscous and buoyancy forces may be rewritten as

$$\frac{1}{\rho}(\mathbf{J}\times\mathbf{B}_0)\cdot\mathbf{u} = -\frac{1}{\rho}(\mathbf{u}\times\mathbf{B}_0)\cdot\mathbf{J} = -\frac{J^2}{\sigma\rho} - \nabla\cdot(V\mathbf{J}/\rho)$$

$$-\nu[\mathbf{u}\cdot(\nabla\times\boldsymbol{\omega})] = -\nu\left\lfloor\omega^2 + \nabla\cdot(\boldsymbol{\omega}\times\mathbf{u})\right\rfloor$$

$$g\beta(Tu_z) = g\beta(\delta Tu_z + \Delta T(1 - z/d)u_z)$$

$$= g\beta\left\lfloor\delta Tu_z + \nabla\cdot\left((z - z^2/2d)\Delta T\mathbf{u}\right)\right\rfloor$$

where δT is the (small) departure of T from the static, linear distribution. We now gather all the divergence terms together and rewrite our energy equation as

$$\frac{\partial}{\partial t}\left(\frac{u^2}{2}\right) = \nabla\cdot(*) - \frac{J^2}{\sigma\rho} - \nu\omega^2 + g\beta u_z\delta T$$

Now the divergence term vanishes when this equation is integrated over the entire pool (or a single convection cell) and we obtain

$$\frac{d}{dt}\int\left(\frac{u^2}{2}\right)dV = -\frac{1}{\rho\sigma}\int J^2dV - \nu\int\omega^2dV + g\beta\int u_z\delta TdV$$

The dissipative rôles of the viscous and Lorentz forces are now apparent, as is the source of potential energy, $g\beta\delta Tu_z$. We would expect that the equilibrium is unstable wherever the fluid can arrange for

$$g\beta\int u_z\delta TdV \geq \frac{1}{\rho\sigma}\int J^2dV + \nu\int\omega^2dV$$

with marginal stability corresponding to the equality sign. Let us now try to estimate the various integrals above. Suppose that the convection cells are two-dimensional, taking the form of rolls, with $\mathbf{u}$ confined to the x–z plane. We might approximate the shape of these by the streamfunction $\psi(\mathbf{x}, t) = \hat{\psi}(t)\sin(\pi z/d)\sin(\pi x/l)$, where $2l$ is the wavelength of the instability. Also, we suppose the onset of the instability to be non-oscillatory, so that $s = 0$ at $Ra = (Ra)_c$. (All of the experimental and analytical evidence suggests that this is the case, except perhaps in certain hot plasmas in which $\nu > \lambda$.) Since the electrostatic potential, V, is zero for two-dimensional flow, (5.4) gives, for one cell,

$$\frac{1}{\rho\sigma}\int J^2dV = \left(\frac{\sigma B_0^2}{\rho}\right)\int u_x^2dV = \left(\frac{\sigma B_0^2}{\rho}\right)\left(\frac{\pi}{2d}\right)^2\hat{\psi}^2ld$$

The viscous dissipation, on the other hand, takes the form

$$\nu \int \omega^2 dV = (\nu/4)\left[(\pi/l)^2 + (\pi/d)^2\right]^2 \hat{\psi}^2 ld$$

Finally, the buoyancy integral can be estimated with the aid of $(\mathbf{u} \cdot \nabla)T_0 = \alpha \nabla^2(\delta T)$, which yields

$$\delta T = \alpha^{-1}\nabla^{-2}(\mathbf{u} \cdot \nabla T_0) = \alpha^{-1}\left[(\pi/l)^2 + (\pi/d)^2\right]^{-1} u_z(\Delta T/d)$$

where $f = \nabla^{-2}g$ is a symbolic representation of $g = \nabla^2 f$. This gives the estimate

$$g\beta \int \delta T u_z dV = g\beta\alpha^{-1}\left[(\pi/l)^2 + (\pi/d)^2\right]^{-1}(\Delta T/d)(\pi/2l)^2 \hat{\psi}^2 ld$$

Thus the transition to instability occurs when

$$\underbrace{\left[\frac{g\beta\Delta T d^3}{\alpha}\right]\frac{(\pi/l)^2}{\left[(\pi/l)^2 + (\pi/d)^2\right]}}_{\text{(driving force)}} = \underbrace{\pi^2\left[\frac{\sigma B_0^2 d^2}{\rho}\right]}_{\text{(Joule dissipation)}} + \underbrace{\nu\left[\pi^2 + \left(\frac{\pi d}{l}\right)^2\right]^2}_{\text{(viscous dissipation)}}$$

Introducing the cell aspect ratio, $a = (\pi d/l)$, this simplifies to

$$(Ra)_c = a^{-2}\left(a^2 + \pi^2\right)\left\{(\pi^2 + a^2)^2 + \pi^2(Ha)^2\right\}$$

where $Ha = (\sigma B_0^2 d^2/\rho\nu)^{1/2}$ is the Hartmann number introduced in Chapter 3. It remains to estimate a. We now suppose that the cell shape is chosen so as to maximise the rate of working of the buoyancy force and minimise the dissipation. That is to say, we choose l/d such that $(Ra)_c$ is a minimum. This yields

$$(2a^2 - \pi^2)(a^2 + \pi^2)^2 = \pi^4(Ha)^2$$

from which we find

$$Ha \to 0: \qquad a = 2.22, \qquad (Ra)_c = 675$$

$$Ha \to \infty: \qquad a = (\pi^4/2)^{1/6}(Ha)^{1/3}, \qquad (Ra)_c = \pi^2(Ha)^2$$

Note that, for $Ha = 0$, the convection rolls are predicted to have an aspect ratio d/l of the order of unity, while the cells are narrow and deep at high Ha. We have made many assumptions in deriving these criteria, and so we must now turn to the exact analysis to see how our guesses have faired. Fortuitously it turns out that our estimate of $(Ra)_c$ at large Ha is exactly correct! Our estimate of $(Ra)_c = 675$ at $Ha = 0$ is less good though. Depending on the boundary conditions at $z = 0$ and d, an

exact analysis gives $(Ra)_c = 658$ (two free surfaces), 1100 (one free, one solid) and 1708 (two solid surfaces). Still, our energy analysis seems to have caught the essence of the process, and it is satisfying that its predictions are exact at high *Ha*. (The errors at low *Ha* are due to the assumed distribution of ψ.) It would seem that the cell size automatically adjusts to give the best possibility of an instability, minimising dissipation while maximising the rate of working of the buoyancy flow.

5.4.4 Natural convection in other configurations

The Rayleigh–Bénard configuration represents a singular geometry in the sense that it admits a static solution of the governing equations (uniform conduction, $\mathbf{u} = 0$). Convection appears only because this solution is unstable at high values of ΔT or low values of ν. In most geometries (for example a heated plate whose flat faces are vertical) motion develops irrespective of the size of ν and ΔT. There is no static solution of the governing equations. In such cases the smallest temperature difference will drive motion. The influence of an imposed magnetic field is then different. It does not delay the onset of convection, as in the Rayleigh–Bénard geometry, but rather moderates the motion which inevitably occurs.

Consider the case of a vertical plate held at a temperature ΔT above the ambient fluid temperature. Here the motion is confined to a thermal boundary layer, δ, which grows from the base of the plate as the fluid passes upwards. When there is no imposed field we can estimate u and δ from the equations

$$u(\partial u/\partial z) \sim g\beta\Delta T \qquad \text{(vertical equation of motion)}$$

$$u(\partial T/\partial z) \sim \alpha T/\delta^2 \qquad \text{(heat balance)}$$

This yields

$$u \sim (g\beta\Delta T z)^{1/2}$$

$$\delta \sim (g\beta\Delta T/\alpha^2)^{-1/4} z^{1/4}$$

where z is measured from the base of the plate. (Actually, these estimates are accurate only for low Prandtl number fluids, $\nu/\alpha \ll 1$, such as liquid metals. When the Prandtl number is of order unity, or greater, the viscous term $\nu u/\delta^2$ must be included in the vertical force balance, leading to a modification in the estimate of δ. However, we shall stay with liquid metals for the moment.) Let us see how magnetic damping alters the

situation. The imposition of a horizontal magnetic field, B, modifies the first of these equations to

$$u(\partial u/\partial z) \sim g\beta\Delta T - u/\tau, \qquad \tau^{-1} = \sigma B^2/\rho$$

Evidently, the fluid ceases to accelerate when u reaches a value of u^* given by

$$u^* \sim (g\beta\Delta T)\tau$$

For a plate of length l, the ratio of $u_{\max}$ with and without a magnetic field is therefore

$$\frac{u^*}{u} \sim \frac{(g\beta\Delta Tl)^{1/2}}{\sigma B^2 l/\rho} \sim \frac{(Ra)^{1/2}(\alpha/\nu)^{1/2}}{Ha^2}$$

so that the damping effect goes as $\sim B^2$. (The expression above assumes τ is small enough, or l large enough, for u to saturate before it leaves the plate.) For efficient damping, therefore, we require

$$Ha^2 \geq (Ra)^{1/2}(\alpha/\nu)^{1/2}$$

The use of magnetic fields to curtail unwanted natural convection is quite common. For example, in the casting of aluminium, the natural convection currents in a partially solidified ingot are significant (a few cm/s), and are thought to be detrimental to the ingot structure, causing a non-uniformity of the alloying elements through the transport of crystal fragments. Static magnetic fields have been used to minimise this natural convection. In the laboratory, on the other hand, the standard method of measuring the thermal diffusivity of liquid metals relies on injecting heat into the metal and measuring the rate of spread of heat by conduction. However, natural convection disrupts this procedure, and since it is difficult to design an apparatus free from convection, magnetic damping is employed to minimise the flow. Convection in a magnetic field is also important in geophysics and astrophysics. The terrestrial magnetic field is maintained by motion in the liquid core of the earth and this is driven, in part, by solutal and thermal convection. However, this convection is damped by the terrestrial field (see Chapter 6). Finally, in the outer layers of the sun, heat is transferred from the interior to the surface by natural convection, and in the case of sunspots this happens in the presence of a significant magnetic field. There are many other applications of magnetoconvection and it is not surprising, therefore, that this subject is receiving much attention at the present time.

Part 2: Generation of Motion

5.5 Rotating Fields and Swirling Motions

5.5.1 Stirring of a long column of metal

Let us now consider a problem which frequently arises in engineering. This illustrates the capacity for magnetic fields to induce motion as well as suppress it. Suppose that fluid is held in a long cylinder of radius R and that a uniform magnetic field rotates about the cylinder with angular velocity Ω as shown in Figure 5.5. In effect, we have a simple induction motor, with the fluid playing the rôle of rotor. The rotating magnetic field therefore induces an azimuthal velocity, $u_\theta(r)$, in the fluid, stirring the contents of the cylinder.

The use of magnetic stirring is very common in the continuous casting of steel. Here, alloying elements tend to segregate out of the host metal during solidification, giving rise to inhomogeneity in the final ingot. Moreover, small cavities can form in the ingot either because of trapped gas or because of the shrinkage of the metal during freezing. All of these defects can be alleviated by stirring the liquid pool.

We now try to estimate the magnitude of the induced velocity. Let us start by evaluating the Lorentz force. For simplicity, we suppose that the field rotation rate is low (in the sense that $\Omega R \ll \lambda/R$). Next we change frames of reference so that the field is stationary. The fluid then appears to rotate in a clockwise direction at a rate $\hat{u} = (\Omega r - u_\theta)$. We now satisfy the low-R_m conditions of Section 5.1 and so

$$\mathbf{J} = \sigma(-\nabla V + \hat{\mathbf{u}} \times \mathbf{B}), \qquad \mathbf{F} = \mathbf{J} \times \mathbf{B} \tag{5.25a, b}$$

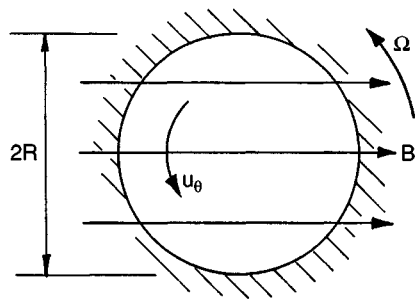

Figure 5.5 Magnetic stirring using a rotating magnetic field.

Now the divergence of (5.25a) gives us $\nabla^2 V = 0$, and so we may take $V = 0$ provided that no electrostatic field is applied at the boundaries. It follows that

$$\mathbf{F} = \mathbf{J} \times \mathbf{B} = \sigma(\hat{\mathbf{u}} \times \mathbf{B}) \times \mathbf{B} = -\sigma B^2 \hat{\mathbf{u}}_\perp \tag{5.26}$$

In (r, θ) coordinates this becomes

$$\mathbf{F} = \sigma B^2 (\Omega r - u_\theta) \cos\theta (\sin\theta, \cos\theta)$$

which may be conveniently split into two parts:

$$\mathbf{F} = \frac{1}{2}\sigma B^2 (\Omega r - u_\theta)\hat{\mathbf{e}}_\theta + \frac{1}{4}\sigma B^2 (\Omega - u_\theta / r)\nabla(r^2 \sin 2\theta) \tag{5.27}$$

Now, although we have assumed that $\Omega R \ll \lambda / R$ (i.e. $\mu\sigma\Omega R^2 \ll 1$), it may be shown that expression (5.27) is a good approximation up to values of $\mu\sigma\Omega R^2 \sim 1$, with a maximum error of $\sim$4%. (There is some hint of this in Figure 4.6, which shows very little field distortion at $R_m = 1$.) It turns out that this is useful since most engineering applications are characterised by the double inequality

$$u_\theta \ll \Omega R \leq \lambda / R$$

and so, for most practical purposes, we may take

$$\mathbf{F} = \frac{1}{2}\sigma B^2 \Omega r \hat{\mathbf{e}}_\theta + \nabla\phi, \qquad \phi = \frac{1}{4}\sigma B^2 \Omega r^2 \sin 2\theta$$

The second term may now be dropped since ϕ simply augments the pressure distribution in the fluid and plays no rôle in the dynamics of the flow. Finally we end up with

$$\mathbf{F} = \frac{1}{2}\sigma B^2 \Omega r \hat{\mathbf{e}}_\theta$$

We now consider the equations of motion for the fluid. The radial component of the Navier–Stokes equation simply expresses the balance between $\partial p / \partial r$ and the centripetal acceleration. The azimuthal component gives, in the steady state,

$$\tau_{r\theta} r^2 = -\int_0^r r^2 F_\theta dr$$

This represents the torque balance on a cylinder of radius r (Figure 5.6). Substituting for $\tau_{r\theta}$ using Newton's law of viscosity yields

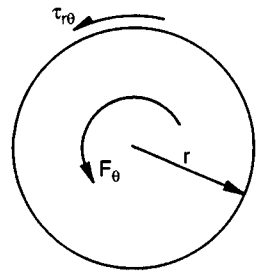

Figure 5.6 Torque balance between the Lorentz force and viscous stresses

$$\tau_{r\theta} = \rho\nu r \frac{d}{dr}\left(\frac{u_\theta}{r}\right) = -\frac{1}{8}\sigma B^2 \Omega r^2 \tag{5.28}$$

which may be integrated to give

$$u_\theta / r = \frac{\sigma B^2 \Omega}{16\rho\nu}\left(R^2 - r^2\right) \tag{5.29}$$

Unfortunately (5.29) is of little practical value since very few flows of this type are laminar. The viscosity, ν, of most liquid metals is similar to that of water, and so the Reynolds' number in practical applications is invariably high, implying a turbulent motion. In such cases we must return to (5.28) and replace the laminar shear stress by the turbulent *Reynolds stress* which appears in the time-averaged equations of motion for a turbulent flow (see Section 3.6). This gives

$$\tau_{r\theta} = -\overline{\rho v_r v_\theta} = -\frac{1}{8}\sigma B^2 \Omega r^2 \tag{5.30}$$

where v represents the fluctuating component of velocity and the overbar denotes a time average. We now need some means of estimating the Reynolds stress. As noted in Section 3.6, a commonly used, although ultimately empirical, model for turbulent shear flows is Prandtl's *mixing length* model. The essence of this model is that we approximate the Reynolds' stress in a planar flow adjacent to a wall by

$$\tau_{xy} = \rho l_m^2 \left|\frac{\partial \bar{u}_x}{\partial y}\right| \frac{\partial \bar{u}_x}{\partial y}, \qquad l_m = \kappa y$$

where $\bar{u}_x$ is the time-averaged velocity, l_m is called the mixing length, and y is the distance from the wall. The empirical constant κ is usually taken to be 0.4. The rotational equivalent of this is,

$$\tau_{r\theta} = \rho l_m^2 r^2 \left|\frac{\partial}{\partial r}\left(\frac{\bar{u}_\theta}{r}\right)\right| \frac{\partial}{\partial r}\left(\frac{\bar{u}_\theta}{r}\right), \qquad l_m = \kappa(R - r)$$

Substituting into (5.30) and integrating yields (see example 5.4)

$$(\bar{u}_\theta/r)_{r=0} = \Omega_f \left\{ \frac{1}{2\sqrt{2}\kappa} \ln\left(\frac{\Omega_f R^2}{\nu}\right) + 1.0 \right\} \tag{5.31}$$

where $\Omega_f^2 = \sigma\Omega B^2/\rho$. Note that in a turbulent flow u_θ scales linearly with B (with a logarithmic correction), whereas in a laminar flow u_θ scales as B^2.

Equation (5.31) gives values of $\bar{u}_\theta$ which compare favourably with estimates obtained using more complicated turbulence models. However, its main limitation is the fact that few engineering applications are strictly one-dimensional. The problem is immediately obvious if we refer back to Figure 3.31 showing spin-down of a stirred cup of tea. In a confined domain, rotation invariably induces a secondary flow via Ekman pumping. The inertial forces in the bulk of the fluid are then no longer zero and, in fact, at high values of Re, these forces greatly exceed the shear stresses, even the Reynolds stress. However, (5.31) is based entirely on a balance between $\mathbf{J} \times \mathbf{B}$ and shear, the inertia associated with secondary flow being ignored. Evidently, such a balance is rarely satisfied in practice, and so estimate (5.31) must be regarded with caution.

We shall examine the practical consequences of Ekman pumping in some detail in Chapter 8, where we shall see that (5.31) is often quite misleading. In the meantime, we can gain some hint as to the difficulties involved by considering a second, related example.

5.5.2 Swirling flow induced between two parallel plates

We can gain some insight into the rôle of Ekman pumping by considering a second model problem. This is the MHD analogue of the classical flow shown in Figure 3.32. Suppose we have two infinite, parallel disks located at $z = 0$ and $z = 2w$, and that the gap is filled with liquid metal. The body force $F_\theta = \frac{1}{2}\sigma\Omega B^2 r$ is applied to the fluid inducing a steady, laminar swirling flow. We choose F_θ so that Re is high and look for a steady solution of the Karman type:

$$u_r = \Omega_c r F(z/l)$$
$$u_\theta = \Omega_c r G(z/l)$$
$$u_z = \Omega_c l H(z/l)$$
$$p = \frac{1}{2}\rho\Omega_c^2 r^2 + \rho\Omega_c^2 l^2 P(z/l)$$

Here l is some characteristic length scale, yet to be determined, and Ω_c is a characteristic rotation rate in the core of the flow. We might anticipate that the flow divides into thin Bodewadt layers on the disk surfaces between which lies an inviscid core (Figure 8.4). In fact, this is precisely what happens, as we now show.

Consider the lower half of the flow $0 \leq z \leq w$. Away from the disc we take $l = l_c = w$ (the subscript on l denotes the core flow). In the boundary layer, on the other hand, we try the scaling $l = l_b = (\nu/\Omega_c)^{1/2}$, which is Bodewadt boundary layer scaling. The ratio of these length scales is a sort of inverse Reynolds number,

$$\varepsilon = (\nu/\Omega_c w^2)^{1/2} = l_b/l_c$$

We shall take ε to be vanishingly small and try to match the velocity profiles in the two regions using the method of *matched asymptotic expansions*. Substituting our proposed velocity functions in the Navier–Stokes and continuity equations yields, for both the core and the boundary layer,

$$F^2 + HF' - G^2 + 1 = (\nu/\Omega_c l^2)F'' \qquad \text{(radial equation)}$$

$$2FG + G'H = (\nu/\Omega_c l^2)G'' + \frac{1}{2}\Omega_f^2/\Omega_c^2 \qquad (\theta \text{ equation})$$

$$H' + 2F = 0 \qquad \text{(continuity)}$$

where the prime represents differentiation with respect to z/l and, as before, Ω_f is defined by $\Omega_f^2 = \sigma\Omega B^2/\rho$. In the core of the flow, where $l = l_c = w$, these equations yield (for $\varepsilon \to 0$)

$$F_c^2 + H_c F_c' - G_c^2 = -1$$

$$2F_c G_c + G_c' H_c = \frac{1}{2}\Omega_f^2/\Omega_c^2$$

$$H_c' + 2F_c = 0$$

where again the prime represents differentiation with respect to z/l_c. The boundary conditions for F_c, G_c and H_c arise from the fact that the flow must be symmetric about $z = w$ and that u_z in the core and boundary layer must match at the interface in the sense that

$$\lim_{z/l_c \to 0}[u_z] = \lim_{z/l_b \to \infty}[u_z]$$

This gives

$$z/l_c = 1: \quad H_c = 0, \ F_c' = 0, \ G_c' = 0 \qquad \text{(symmetry)}$$

$$z/l_c \to 0: \quad l_c H_c = l_b H_b(\infty), \text{ or } H_c = \varepsilon H_b(\infty) \qquad \text{(matching condition)}$$

$$z/l_c \to 0: \quad G_c = 1 \qquad \text{(definition of } \Omega_c\text{)}$$

Here $H_b(\infty)$ is the value of H furnished by the boundary-layer solution, while the condition $G_c = 1$ effectively defines Ω_c. Formally

$$H_b(\infty) = \lim_{z/l_b \to \infty} H_b(z/l_b)$$

We now expand F_c, G_c and H_c in polynomials of ε and substitute these into the governing core equations. To leading order in ε we find

$$F_c = \frac{1}{2}\varepsilon H_b(\infty)$$

$$G_c = 1$$

$$H_c = \varepsilon H_b(\infty)[1 - z/w]$$

So the core velocity distribution is

$$\mathbf{u}_c = \left(\frac{1}{2}\varepsilon H_b(\infty)\Omega_c r, \Omega_c r, \varepsilon H_b(\infty)\Omega_c[w - z]\right)$$

Note that we have rigid-body rotation in the core and that u_r and u_z are of order $\sim \varepsilon u_\theta$. It appears that, for small ε, the core velocity is determined by only three parameters: ε, Ω_c and $H_b(\infty)$. The second of these, Ω_c, is fixed by the azimuthal component of the core equation of motion, which may be rearranged to give

$$\Omega_c = \Omega_f\left[\Omega_f w^2/\nu\right]^{1/3}[2H_b(\infty)]^{-2/3}$$

It now remains to find $H_b(\infty)$, and this is furnished by the boundary-layer equations. Immediately adjacent to the disk, the azimuthal equation of motion becomes

$$2F_b G_b + G_b' H_b = G_b'' + \frac{1}{2}\Omega_f^2/\Omega_c^2$$

where the prime now represents differentiation with respect to z/l_b. However, we have already shown that the last term on the right of this equation is of order ε. Consequently, magnetic forcing is negligible in the boundary layer (by comparison with viscous and inertial forces) and the equations locally reduce to those for a conventional Bodewadt layer, for which $H_b(\infty) = 1.349$. It follows that the core rotation rate is

$$\Omega_c = 0.516\Omega_f \left[\Omega_f w^2/\nu\right]^{1/3}$$

Compare this with our one-dimensional equation for swirl-only flow,

$$\frac{u_\theta}{r} = \frac{\Omega_f}{16}\left[\frac{\Omega_f R^2}{\nu}\right]\left[1 - \left(\frac{r}{R}\right)^2\right]$$

The dependence of u_θ on B is entirely different in the two cases, reflecting the different force balances. In the swirl-only flow, $\mathbf{J} \times \mathbf{B}$ is balanced by shear. In this second problem the primary balance in the core of the flow is between $\mathbf{J} \times \mathbf{B}$ and Coriolis forces. (This may be confirmed by tracing the origin of the terms in the azimuthal equation of motion.)

So this simple swirling flow is more complex than you might think! There are subtle and unexpected effects introduced by Ekman pumping. We shall return to this issue in Chapter 8, where we show that the balance between $\mathbf{J} \times \mathbf{B}$ and Coriolis forces is, in fact, typical of most flows encountered in practice.

5.6 Motion Driven by Current Injection

There is a second way of driving motion in a conducting fluid. So far we have considered only currents which are induced in the fluid by rotation of the magnetic field. However, we can also inject current directly into a fluid, and the resulting Lorentz force will, in general, produce motion. The simplest example of this is the electromagnetic pump, which was described in Chapter 1. Such a device consists of a duct in which mutually perpendicular magnetic and electric fields are arranged normal to the axis of the duct. The resulting Lorentz force, $\mathbf{J} \times \mathbf{B}$, is directed along the axis of the duct and this can be used to pump a conducting fluid. For example, sodium coolant is pumped around fast breeder nuclear reactors by this method. It turns out, however, that an understanding of this flow comes down to a careful consideration of the boundary layers, and so we shall postpone any discussion of this problem until the next section. Here we consider a configuration related to electric welding. The discussion is brief, but we shall return to this problem in Chapter 10.

5.6.1 A model problem

A useful model problem is the following. Suppose we have a liquid-metal pool which is hemispherical in shape, of radius R. The boundaries are

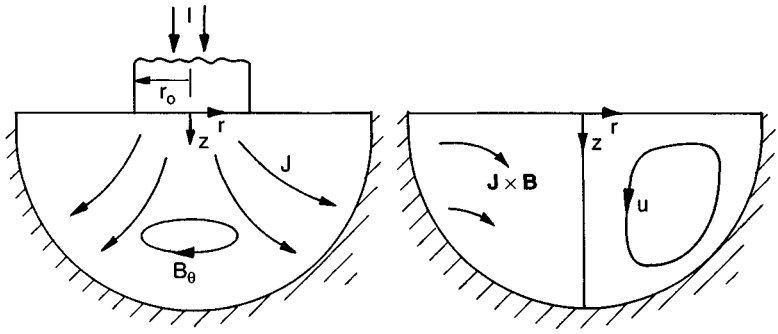

Figure 5.7 Geometry of the model problem.

assumed to be conducting and a current, I, is introduced into the pool by an electrode of radius r_0, which touches the surface. The entire geometry is axisymmetric and we use cylindrical polar coordinates (r, θ, z) with the origin at the pool's surface, as shown in Figure 5.7. The poloidal current gives rise to an azimuthal field, B_θ, and the two are related by Ampère's law, according to which

$$2\pi r B_\theta = \mu \int_0^r (2\pi r J_z) dr$$

The interaction of $\mathbf{J}$ with B_θ gives rise to a Lorentz force, and it is readily confirmed that

$$\mathbf{F} = \mathbf{J} \times \mathbf{B}/\rho = -\nabla(B_\theta^2/2\rho\mu) - \left\lfloor B_\theta^2/(\rho\mu r)\right\rfloor \hat{\mathbf{e}}_r$$

Of course, the magnetic pressure merely augments the fluid pressure and does not influence the motion in the pool. We therefore write

$$\mathbf{F} = -\frac{B_\theta^2}{\rho\mu r}\hat{\mathbf{e}}_r$$

on the understanding that p is augmented by $B_\theta^2/(2\mu)$. Clearly, this Lorentz force will drive a recirculating flow which converges at the surface (where B_θ is largest) and diverges near the base of the pool. The question is: can we estimate the magnitude of the induced flow?

5.6.2 *A useful energy equation*

We now describe a useful trick which we shall employ repeatedly in the subsequent chapters. Whenever we wish to estimate the recirculating flow

induced by a prescribed Lorentz force, it is useful to integrate the Navier–Stokes equation

$$\frac{\partial \mathbf{u}}{\partial t} = \mathbf{u} \times \boldsymbol{\omega} - \nabla\left[\frac{p}{\rho} + \frac{u^2}{2}\right] + \nu\nabla^2\mathbf{u} + \mathbf{F}$$

once around a closed streamline, C. In the steady state this yields

$$\oint_C \mathbf{F} \cdot d\mathbf{l} = -\nu \oint_C \nabla^2\mathbf{u} \cdot d\mathbf{l}$$

since $(\mathbf{u} \times \boldsymbol{\omega}) \cdot d\mathbf{l} = 0$ and the gradient of Bernoulli's function integrates to zero. Evidently there must be a global balance between the Lorentz force and the shear stresses. Physically, this arises because the work done by $\mathbf{F}$ on a fluid particle as it passes once around the streamline must be balanced by the (dissipative) work performed by the shear stresses acting on the same particle. If the two did not match, then the kinetic energy of the fluid particle would not be the same at the beginning and end of the integration, which is clearly not the case in a steady flow. We may use this integral equation to estimate $|\mathbf{u}|$.

Let us see where this leads in our model problem. We take C to be the bounding streamline, comprising the surface, the axis and the curved boundary. Starting with the left-hand integral we have

$$\oint \mathbf{F} \cdot d\mathbf{l} = \left[\int_0^R (B_\theta^2/\rho\mu r)dr\right]_{z=0} - \left[\int_0^R (B_\theta^2/\rho\mu r)dr\right]_{r^2+z^2=R^2}$$

The first of these integrals is readily evaluated since, from Ampère's law, $2\pi r B_\theta = \mu I(r/r_0)^2$ for $r < r_0$ and $2\pi r B_\theta = \mu I$ for $r > r_0$. This yields

$$\left[\int_0^R (B_\theta^2/\rho\mu r)dr\right]_{z=0} = \frac{\mu I^2}{4\pi^2\rho r_0^2}\left[1 - (r_0^2/2R^2)\right]$$

The second integral is more difficult. However, if $r_0 \ll R$ then the field in the vicinity of the boundary is that due to a point source of current, and the corresponding field is readily shown to be

$$2\pi r B_\theta = \mu I\left[1 - z\Big/\left(r^2 + z^2\right)^{1/2}\right], \qquad (r_0 \ll R)$$

This yields

$$\left[\int_0^R (B_\theta^2/\rho\mu r)dr\right]_{r^2+z^2=R^2} = \frac{\mu I^2}{4\pi^2\rho R^2}[\ln 2 - 1/2]$$

Combining these expressions gives us

$$\oint \mathbf{F} \cdot d\mathbf{l} = \frac{\mu I^2}{4\pi^2 \rho}\left[\frac{1}{r_0^2} - \frac{\ln 2}{R^2}\right] = -\nu \oint \nabla^2 \mathbf{u} \cdot d\mathbf{l}$$

For cases where r_0 does not satisfy $r_0 \ll R$ the factor of $\ln 2$ above will need modification. However, the details do not matter. The main point is that

$$\frac{\mu I^2}{4\pi^2 \rho r_0^2} \sim -\nu \oint \nabla^2 \mathbf{u} \cdot d\mathbf{l}$$

Although we have performed the integration only for the bounding streamline, a similar relationship must hold for all streamlines which pass close to the electrode. For streamlines remote from the electrode we would expect

$$\frac{\mu I^2}{4\pi^2 \rho R^2} \sim -\nu \oint \nabla^2 \mathbf{u} \cdot d\mathbf{l}$$

since r_0 ceases to be a relevant dimension in such cases. We can use these equations to estimate $|\mathbf{u}|$.

5.6.3 Estimates of the induced velocity

Suppose that the Reynolds number is not too high, say somewhat less than 100. Then there are no significant boundary layers on the outer wall. (Such layers usually start to form when $\mathrm{Re} > \sim 100$.) The only region where high velocity gradients will form is near the electrode where the characteristic gradient in $\mathbf{F}$ is $|\mathbf{F}|/r_0$, and so we would expect local gradients in $\mathbf{u}$ to be of the order of $|\mathbf{u}|/r_0$. Elsewhere we would expect $\nabla^2\mathbf{u}$ to scale as $|\mathbf{u}|/R^2$. If these statements are true, then our integral equations suggest that

$$u \sim \frac{\mu I^2}{4\pi^2 \rho \nu r_0} \qquad \text{(near electrode)}$$

$$u \sim \frac{\mu I^2}{4\pi^2 \rho \nu R} \qquad \text{(elsewhere)}$$

Somewhat surprisingly these scalings turn out to be valid (provided Re is not too large), as we shall see in Chapter 10.

We end this section by considering the highly idealised case where the outer boundary is removed and $r_0 \to 0$, so that we have a point electrode located on the surface of a semi-infinite fluid. Of course, this is of little practical significance, but it has been the subject of considerable attention

in the literature because it turns out that there is an exact, self-similar, solution for this flow. This solution is of the form

$$u \sim \frac{\mu I^2}{4\pi^2 \rho \nu (r^2 + z^2)^{1/2}} g(\phi, \mathrm{Re})$$

(see suggested reading at the end of this chapter), where ϕ is the angle between the z-axis and the position vector, $\mathbf{x}$, and g is a function of ϕ and of $\mathrm{Re} = u|\mathbf{x}|/\nu$. The similarity to our estimates above is reassuring. However, it would be wrong to place too much emphasis on this exact solution since, in many respects, it is atypical. It turns out that the absence of an outer boundary at large $|\mathbf{x}|$ means that the streamlines in this self-similar flow do not close on themselves, but merely converge towards the axis. The flow is therefore free from integral constraints of the form

$$\oint \mathbf{F} \cdot d\mathbf{l} = -\nu \oint \nabla^2 \mathbf{u} \cdot d\mathbf{l}$$

We might anticipate, therefore, that there is a fundamental difference between this self-similar flow and those in which R is large but finite, and we shall confirm this in Chapter 10.

5.6.4 A paradox

We close this section with an apparent paradox. Of course, there are no real paradoxes in science, only confusion in our muddled attempts to understand nature. We shall describe the paradox here and leave the explanation to Chapter 10.

The integral constraint

$$\oint \mathbf{F} \cdot d\mathbf{l} = -\nu \oint \nabla^2 \mathbf{u} \cdot d\mathbf{l}$$

is a very powerful one. It must be satisfied by *every* closed streamline in a steady flow. Now suppose that we make Re large so that boundary layers form on the boundary of the pool. Inside the boundary layers the viscous dissipation is intense, while outside it is small. The boundary layer thickness usually scales as $\delta \sim (\mathrm{Re})^{-1/2} l$, where l is a typical length-scale for the flow, say R. If this is true here, then the integral equation applied to a streamline lying close to the boundary gives

$$|\mathbf{F}| l \sim (\nu |\mathbf{u}| l)/\delta^2 \sim u^2$$

For a streamline away from the boundary, on the other hand,

$$|\mathbf{F}|l \sim (\nu|\mathbf{u}|l)/l^2 \sim \nu|\mathbf{u}|/l$$

Thus the flow in the boundary layer appears to scale as $u \sim (|\mathbf{F}|l)^{1/2}$, while that in the core scales according to $u \sim |\mathbf{F}|l^2/\nu$, which is much greater than $(|\mathbf{F}|l)^{1/2}$ when Re is large. However, this cannot be so, since the velocity scale in the boundary layer is set by the velocity in the core. Clearly, there is a mistake somewhere! (The mistake is not in the estimate of δ.) Physically, this paradox arises because the fluid in the boundary layer appears to receive significant dissipation, while that in the core is almost inviscid and so, according to previous arguments, larger velocities will develop away from the boundaries.

We will return to this issue in Chapters 8 and 10, where it will be seen that the flow does quite bizarre things in order to satisfy the integral equation.

Example: A false scaling for forced, recirculating flow in a confined domain

Suppose we have a steady laminar, two-dimensional flow, driven by a prescribed Lorentz force, and with a high Reynolds number. The flow is confined to the domain V with the no-slip boundary condition $\mathbf{u} = 0$ on the surface of V. Confirm that, for any streamline C,

$$\oint_C (\mathbf{J} \times \mathbf{B}) \cdot d\mathbf{l} + \rho\nu \oint_C \nabla^2\mathbf{u} \cdot dl = 0$$

The implication is that viscous and magnetic forces are of similar magnitudes. Since $\mathrm{Re} \gg 1$, it follows that inertia greatly exceeds both $\mathbf{J} \times \mathbf{B}$ and $\rho\nu\nabla^2\mathbf{u}$, except in the boundary layers. It follows that, outside the boundary layers, the vorticity is governed by $\mathbf{u} \cdot \nabla\omega \approx 0$, or equivalently, $\omega \approx \omega(\psi)$. Show that

$$\nabla^2\mathbf{u} = -\omega'(\psi)\mathbf{u}$$

and hence confirm that for each streamline which avoids the boundary layers

$$\omega'(\psi) = \oint_C (\mathbf{J} \times \mathbf{B}) \cdot d\mathbf{l} \Big/ \left[\rho\nu \int_A \omega dA\right]$$

where A is the area enclosed by the streamline C. The implication is that $\mathbf{u}$ scales as ν^{-1}. Now show that such a scaling is, in fact, impos-

sible! [Hint: show that this scaling implies an order of magnitude balance between the generation and dissipation of mechanical energy in the core of the flow, which is incompatible with highly dissipative boundary layers.] We appear to have a paradox.

In fact, this is the same paradox as that described above. In practice, the fluid circumvents this dilemma by becoming turbulent at rather low Reynolds numbers (of ~ 100), or else by forcing all of the streamlines through the dissipative boundary layers so that $\omega \neq \omega(\psi)$ (see Chapter 8).

Part 3: Boundary Layers

5.7 Hartmann Boundary Layers

5.7.1 The Hartmann layer

So far we have considered the influence of $\mathbf{J} \times \mathbf{B}$ on the interior of a flow only. We have not considered its effect on boundary layers. We close this chapter with a discussion of a phenomenon which received much attention in the early literature on liquid-metal MHD: the Hartmann layer. This is often discussed in the context of duct flows, but is really just a boundary-layer effect. The main point is that a steady magnetic field orientated at right angles to a boundary can completely transform the nature of the boundary layer, changing its characteristic thickness, for example.

Suppose we have rectilinear shear flow $u(y)\hat{\mathbf{e}}_x$ adjacent to a plane, stationary, surface. Far from the wall the flow is uniform and equal to u_∞, but close to the wall the no slip condition ensures some kind of boundary layer (Figure 5.8). There is a uniform, imposed magnetic field $\mathbf{B} = B\hat{\mathbf{e}}_y$. Now $\mathbf{B} \cdot \boldsymbol{\omega} = 0$ and so (5.9) tells us $\nabla^2 V = 0$, implying that the electric field is zero. We shall also assume that there is no imposed electric field, and so $V = 0$. It then follows from (5.4) and (5.5) that

$$\mathbf{F} = \mathbf{J} \times \mathbf{B} = -\sigma B^2 u \hat{\mathbf{e}}_x$$

and so we have the usual damping force. The Navier–Stokes equation is now

$$\rho\nu \frac{\partial^2 u}{\partial y^2} - \sigma B^2 u = \frac{\partial p}{\partial x} \tag{5.32}$$

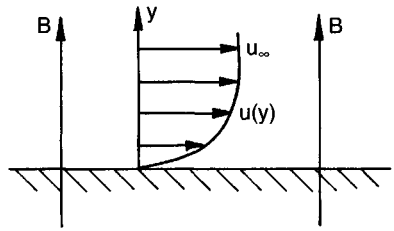

Figure 5.8 A Hartmann flow.

which may be transformed to

$$\frac{\partial^2}{\partial y^2}(u - u_\infty) - \frac{u - u_\infty}{\delta^2} = 0, \qquad \delta = (\rho\nu/\sigma B^2)^{1/2}$$

where u_∞ is the velocity remote from the boundary.

The solution is

$$u = u_\infty\left[1 - e^{-y/\delta}\right] \tag{5.33}$$

We see that the velocity increases rapidly over a short distance from the wall (Figure 5.9). This boundary layer, which has thickness $\sim\delta$, is called a Hartmann layer. Note that the thickness of a Hartmann boundary layer is quite different to that of a conventional boundary layer.

5.7.2 Hartmann flow between two planes

We now consider the same flow, but between two stationary parallel plates located at $y = \pm w$. We also allow for the possibility of an imposed electric field, E_0, in the z-direction. Our equation of motion is now

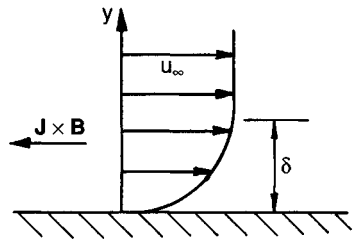

Figure 5.9 The Hartmann boundary layer.

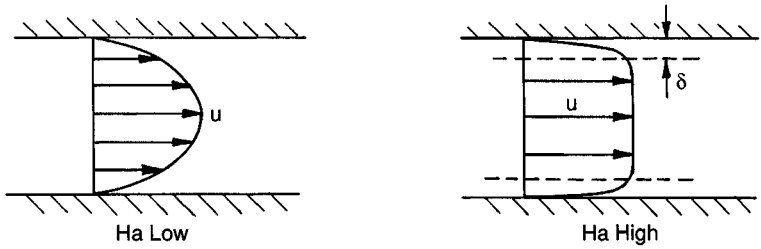

Figure 5.10 Duct flow at low and large Hartmann numbers.

$$\rho\nu\frac{\partial^2 u}{\partial y^2} - \sigma B^2 u = \frac{\partial p}{\partial x} + \sigma B E_0$$

which has the solution,

$$u = u_0\left[1 - \frac{\cosh(y/\delta)}{\cosh(w/\delta)}\right], \qquad \sigma B^2 u_0 = -\frac{\partial p}{\partial x} - \sigma E_0 B$$

It is conventional to introduce the Hartmann number at this point, defined by

$$Ha = w/\delta = Bw(\sigma/\rho\nu)^{1/2}$$

As noted in Section 3.5, $(Ha)^2$ represents the ratio of the Lorentz forces to the viscous forces. Our solution is then

$$u = u_0\left[1 - \frac{\cosh[(Ha)y/w]}{\cosh(Ha)}\right] \tag{5.34}$$

It is instructive to look at the two limits: $Ha \to 0$, $Ha \to \infty$ (Figure 5.10). When Ha is very small we recover the parabolic velocity profile of conventional Poiseuille flow.

$$u = u_0(1 - (y/w)^2)$$

When Ha is very large, on the other hand, we find that exponential Hartmann layers form on both walls, separated by a core of uniform flow. All of the vorticity is pushed to the boundaries.

5.8 Examples of Hartmann and Related Flows

When Ha is large, Hartmann flow is characterised by the three equations

$$u \approx u_0$$

$$J = \sigma(E_0 + u_0 B) \tag{5.35}$$

$$u_0 B = -E_0 - \frac{1}{\sigma B}\frac{\partial p}{\partial x} \tag{5.36}$$

Note that we are free to choose the value of E_0, the external electric field. Depending on how we specify E_0, we obtain quite separate technological devices.

5.8.1 Flow-meters and MHD generators

Suppose we choose $J = 0$, so that $E_0 = -u_0 B$. In this case there is no pressure gradient associated with B, the Lorentz force being zero. Such a device is called an MHD flow-meter since E_0 may be measured to reveal u_0.

Alternatively, if E_0 is zero, or small and positive, we have

$$J \approx \sigma u_0 B, \qquad \left|\frac{\partial p}{\partial x}\right| \approx \sigma B^2 u_0 \tag{5.37}$$

In this case we induce a current, but at the cost of a pressure drop. We are converting mechanical energy into electrical energy plus heat, and such a device is called a generator (Figure 5.11). This is the basis of MHD power generation, where hot ionised gas is propelled down a duct. The technological failure of MHD power generation, which was much publicised in scientific circles, is often attributed to the inability to develop refractory

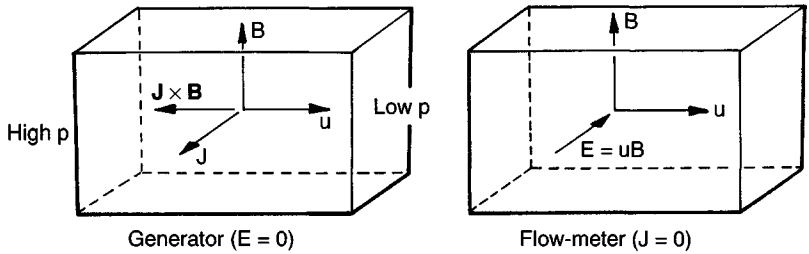

Figure 5.11 Principles of MHD generators and flow-meters.

materials capable of withstanding the high temperatures involved (~ 3000 K), rather than to any flaw in the MHD principle.

5.8.2 Pumps, propulsion and projectiles

If E_0 is negative, and has a magnitude in excess of $u_0 B$, the direction of J (and hence $\mathbf{J} \times \mathbf{B}$) is reversed. In this case dP/dx is positive and we have a pump. Electrical energy is supplied to the device and this is converted into mechanical energy plus heat.

MHD pumps are in common use, both in the metallurgical and the nuclear industries. Their obvious attraction is that they contain no moving parts and so, in principle, they are mechanically reliable. One can even combine a generator with a pump to produce a so-called MHD flow-coupler. Here two ducts sit side by side, one producing electrical power for the other, which acts as a pump. One application is to transfer mechanical energy from one sodium loop to another in fast breeder reactors.

A variant of the MHD pump is the electromagnetic gun, sometimes called a rail gun or electromagnetic launcher. Here there is no applied magnetic field and so this is not a Hartmann flow. Rather, one relies on the field associated with the flow of current along the electrodes and through the fluid (plasma). It is readily confirmed that the interaction of **J** with its self-field **B** induces a Lorentz force parallel to the electrodes (Figure 5.12). This is used to propel a plasma ahead of which sits a non-conducting projectile. The advantage of such a device is that, as long as current is supplied, the projectile will accelerate. This contrasts with conventional chemical guns where movement of the projectile is

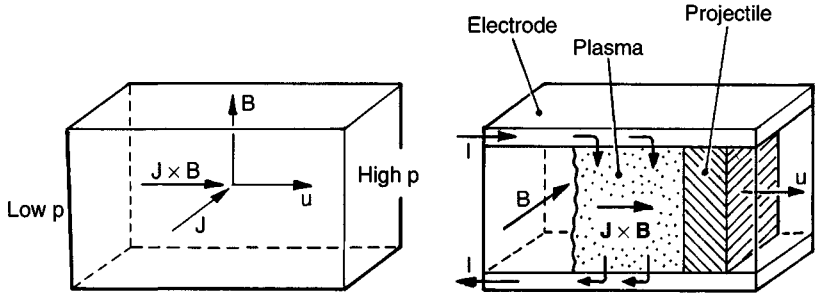

Figure 5.12 Principles of MHD pumps and guns.

associated with an expansion of the gas and hence a loss in pressure. Small masses have been accelerated up to speeds of around 7 km/s in such devices.

Typically the electrodes are connected to a capacitor bank which delivers a current pulse of around $10^5 \rightarrow 10^6$ Amps in a period of a few milliseconds. In the first instance this vaporises a metal foil placed between the electrodes (rails) and so initiates a plasma. Current then enters the top rail, is syphoned off through the plasma and returns via the bottom rail. The resulting force accelerates the plasma along the duct, pushing the projectile ahead of it.

This simple idea is attractive to the extent that it can produce velocities much higher than those achievable by conventional means. It has been suggested that it might be used in fusion research, to create high impact velocities, as a laboratory tool to study high velocity projectiles and, of course, it has military applications. However, in practice it has three major drawbacks. First, the electrical power involved is substantial and this has to be delivered in a very short pulse. Considerable attention must be paid, therefore, to the storage and delivery of the electrical power. Second, the magnetic repulsion forces between the rails is very large, and great care is required in the mechanical design of the gun, otherwise it is prone to self-destruct! Third, the plasma temperatures are very high, $\sim 2.5 \times 10^4$ K, and so there is a severe ablation of material from the inside surface of the duct. As a consequence, the plasma grows rapidly in size and weight, increasing the inertia of the propelled mass and reducing the projectile acceleration.

A variant of the electromagnetic gun, in which the projectile is removed, is the electromagnetic jet thruster. Here the device operates continuously: heating, ionising and propelling a plasma. Typically this has an annular geometry with a central cathode surrounded by a cylindrical anode. The gas is accelerated down the annular gap between the two, producing thrust. This has been proposed as a means of propelling space vehicles, its perceived advantages being its low fuel consumption.

There are many other variants of electromagnetic pumps and thrusters, including the much-publicised, but ill-fated, sea-water thruster for submarines. Some, such as the liquid-metal pump, are in common use. Others, such as the electromagnetic launcher, have yet to find any significant commercial application. In general it seems that the simplest, almost mundane, applications have faired best, while the more exotic suggestions have not been realised.

5.9 Conclusion

We have seen that, because of Joule dissipation, an imposed, static magnetic field tends to dampen out fluid motion, while simultaneously creating a form of anisotropy, in which the gradients in **u** parallel to **B** are preferentially destroyed. Thus turbulence in the presence of a strong magnetic field becomes quasi-two-dimensional as the eddies elongate in the direction of **B**. Travelling or rotating magnetic fields, on the other hand, tend to induce a motion which reduces the relative speed of the field and fluid. The magnitude of the induced velocity is controlled by friction. Finally we have shown that magnetic fields alter the structure of boundary layers, which are now controlled by the competition between Lorentz forces and shear. All in all, it seems that magnetic fields provide a versatile, non-intrusive, means of controlling liquid-metal flows.

Suggested Reading

J A Shercliff, *A Textbook of Magnetohydrodynamics*, 1965, Pergamon Press (Chapter 6).

R Moreau, *Magnetohydrodynamics*, 1990, Kluwer Acad. Pub. (Chapter 4 for Hartmann layers, Chapter 5 for damping of jets, Chapter 6 for rotating flow and for the point electrode problem.)

S Chandrasekhar, *Hydrodynamic Stability*, 1981, Dover. (Chapters 2 and 4 for Bénard convection.)

Examples

5.1 Consider the MHD jet shown in Figure 5.2(b). The imposed magnetic field is weak, in the sense that axial gradients in u are much smaller than the transverse gradient. Sketch the induced current distribution at any one cross section of the jet and estimate, qualitatively, the distribution of $\mathbf{J} \times \mathbf{B}$. Explain why the jet elongates in the direction of **B** and also explain why a reverse flow is induced.

5.2 Consider the vortex shown in Figure 5.3(b). Sketch the induced current distribution (which is poloidal) and estimate, qualitatively, the distribution of $\mathbf{J} \times \mathbf{B}$. Show that this force induces a counter rotation in an annulus which surrounds the primary vortex.

5.3 Consider the inviscid flow shown in Figure 5.4(a). Show that the result $\mathbf{H}_{//} =$ constant is not restricted to low values of N. (Hint, the interaction of **J** with its self-magnetic field can give rise to no net torque on the fluid.)

5.4 The integration of (5.30) using the mixing length model of turbulence yields

$$u_\theta/r\Omega_f = \left(2\sqrt{2}\kappa\right)\ln(R-r) + \text{constant}$$

The constant of integration is determined by the fact that, near the wall, the velocity profile must blend smoothly into the universal law of the wall:

$$\bar{u}/u^* = \kappa^{-1}\ln(u^* y/\nu) + 5.5, \qquad y = R - r$$

where $u^* = (\tau_w/\rho)^{1/2}$ is the shear velocity. This yields (5.31). When the surface is rough, however, the universal law of the wall changes to

$$\bar{u}/u^* = \kappa^{-1}\ln(y/k^*)$$

where k^* is the roughness height. Under these circumstances, show that (5.31) must be modified to

$$(\bar{u}_\theta/r)_0 = \Omega_f\left(2\sqrt{2}\kappa\right)^{-1}\ln(R/k^*)$$

5.5 When liquid metal is stirred in a hemispherical container by an azimuthal Lorentz force, Ekman layers are set up on the boundaries. Sketch the secondary flow induced by Ekman pumping.